Polymer 354 (2026) 129894

Contents lists available at ScienceDirect

Polymer

journal homepage: www.elsevier.com/locate/polymer

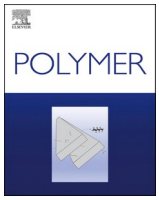

Crystal to condis-crystal transition in poly(VDF-*co*-TrFE) copolymers studied by NMR and SAXS-WAXS

Sara Zanchi [a], Sami Zeliouche [b], Vincent Ladmiral [b], Gilles Silly [b], Fabrice Domingues Dos Santos [c], Béatrice Allard-Breton [d], Sylvie Tencé-Girault [a,e], Sébastien Roland [a,*]

[a] *Laboratoire PIMM, Arts et Metiers Institute of Technology, CNRS, Cnam, 151 boulevard de l'Hopital, 75013, Paris, France*
[b] *ICGM, University of Montpellier, CNRS, ENSCM, Montpellier, France*
[c] *Piezotech S.A.S., Arkema - CRRA, Rue Henri Moissan, Pierre-Bénite Cedex, 69493, France*
[d] *Arkema, CRRA, Rue Henri Moissan, Pierre-Bénite Cedex, 69493, France*
[e] *Arkema, CERDATO, Route du Rilsan, Serquigny, 27470, France*

ARTICLE INFO

Keywords:
VDF based copolymer
Crystal-crystal transition
Solid state NMR
SAXS-WAXS
Dielectric spectroscopy

ABSTRACT

The relationship between chain mobility and semi-crystalline organization of two P(VDF-*co*-TrFE) copolymers with 65/35 and 46/54 VDF/TrFE ratios was studied by combining various experimental techniques (DSC, SAXS-WAXS, and solid-state NMR). This allowed to associate low-density crystalline phases, such as the relaxor ferroelectric (RFE) and the paraelectric (PE) ones, with high molecular mobility, close to the mobility of the amorphous phase. Conversely, the high-density ferroelectric (FE) and defective ferroelectric (DFE) phases, were found to have low and comparable mobility, which decreases after polarization. Moreover, the PE hexagonal phase was investigated, its representation was found to be consistent with the description of condis phase made by Wunderlich in the late 80s. Indeed, the PE hexagonal phase, obtained through a 1st or 2nd order transition (from the FE and RFE phases, respectively), was confirmed to exhibit a long-range positional and orientational order, but with dynamic conformational disorder and high molecular mobility.

1. Introduction

Poly(vinylidene fluoride) (PVDF) is a semi-crystalline polymer studied for many years, in particular for its very rich polymorphism and for its unique and specific properties such as ferroelectricity and piezoelectricity [1–4]. These properties are associated with the orthorhombic pseudo-hexagonal β phase in which chains are in all-*trans* conformations. Many studies have focused on the PVDF polymorphism and the stability of its different phases, in particular the most common orthorhombic α phase, in which chains are in *trans-gauche*$^+$ and *trans--gauche*$^-$ conformations (TG^+ and TG^-) and the most important, for ferroelectric properties, β phase (all-*trans*) [1]. During polymerization, « head-to-head » (H–H) (CF_2-CF_2 sequences) or « tail-to-tail » (T−T) (CH_2–CH_2 sequences) units can arise in the backbone. The impact of these defects on molecular conformations has been studied by Lando et al. [5] Depending on their amount, they can incorporate the crystalline phase and induce a transition from the α phase to the β phase explained by steric considerations [5,6]. A smooth progression from the α phase, to a mixture of α and β, and to a β phase has been observed for H–H/T−T defects amounts varying from 0 mol% to 15 mol% [7]. These defects are sterically equivalent to tetrafluoroethylene (TFE) or trifluoroethylene (TrFE) repetitive units being incorporated next to a VDF repetitive unit [5]. It is therefore the reason why P(VDF-*co*-TrFE) copolymers are still under study and used in numerous applications [8]. For P(VDF-*co*-TrFE), the phase diagram was determined over the whole composition range [9]. With a VDF content ranging from 65 mol% to 82 mol %, the all-*trans* phase, named LT (for Low-Temperature) [9] or FE (for FerroElectric) [10], can be observed at low temperature. It shows a first-order Curie transition, which leads to a crystalline phase, named HT (High-Temperature) [9] or PE (ParaElectric) [10] at high temperature. For intermediate VDF contents (55 mol %<VDF mol%<65 mol %) or after a first heating above the Curie transition temperature and a subsequent cooling, a defective phase, named CL (CooLed) [9] or DFE (for Defective FerroElectric) [10] is obtained alongside the LT (FE) phase.

* Corresponding author.
E-mail address: sebastien.roland@ensam.eu (S. Roland).

https://doi.org/10.1016/j.polymer.2026.129894
Received 12 February 2026; Received in revised form 19 March 2026; Accepted 21 March 2026
Available online 23 March 2026

These defective crystalline phases contain chains with all-*trans* sequences interrupted by *gauche* (G) conformational defects [10,11]. Finally, with VDF contents below 55 mol%, only the DFE phase (CL) is observed, which is associated with a relaxor ferroelectric behavior [9,12]; this crystalline phase is named RFE [12]. These defective phases (CL, DFE or RFE) show a second-order transition with temperature, which also leads to the HT (PE) phase [9,10]. The high temperature phase is described as a hexagonal structure in which the chains exhibit a partly disordered conformation [13,14] or in which they are conformationally disordered and rotate violently around the chain axis [15]. Depending on the nature of the low temperature phase, i.e., LT (FE) or CL (DFE or RFE), the transition to the HT (PE) phase occurs as a first-order or a second-order transition [9,10,16]. Such transitions have been thoroughly examined by Tashiro et al. [9,11,15], Lovinger et al. [13,14], Tesseydre et al. [16] and Bargain et al. [10].

During the same decades but independently, Wunderlich [17] and Ungar [18] led a reflection with the objective of unifying the treatment of the hexagonal phases in thermotropic polymers. They focused on numerous polymeric systems showing a high temperature hexagonal phase without positional long-range order along the chain direction [17,18]. They proposed a classification of certain thermotropic mesophases and they defined the «condis crystals». These condis phases are characterized by a long-range positional and orientational order but with a dynamic **con**formational **dis**order (condis) [17]. The transition mechanisms leading to this phase were described by Wunderlich [17]. Depending on the concentration of conformational defects in the crystal and their aggregation tendency, Wunderlich demonstrated that the crystal to condis crystal transition can be of the first or the second order, at high or low aggregation tendency, respectively. The aggregation tendency is directly correlated to intermolecular interactions between defect-free chain segments and defective chain segments [17,19]. In their two publications [17,18], P(VDF-*co*-TrFE) copolymers with VDF amount between 50% and 80% are cited for their thermotropic two-dimensional hexagonal phase at high temperature, which is identified as the paraelectric phase.

In the PVDF-based copolymers literature, most authors agree that the high temperature phase (PE) is described as a hexagonal crystalline phase in which chains show a conformational disorder, but they considered a three-dimensional crystal phase. Nonetheless, various interpretations have been published, some authors describe this phase with a random mixture of TT, TG^+, and TG^- conformations [9], which can be distributed over six neighboring sites [20] and some with a 3/1 helical conformation [21–25]. It seems that these conformations sequencing highly depend on the copolymer composition and the concentration of the chemical defects along the chains [21]. The lack of periodicity along the chain axis, underlined by Ungar [18], may explain the different values and descriptions of the c-axis parameter of the PE phase reported in literature [9,20,24–26]. However, for P(VDF-*co*-TrFE) copolymers, this phase is described unanimously as a hexagonal phase, regardless of the TrFE/VDF composition. The crystal-crystal transition was thoroughly studied by Tashiro [9], who analyzed the conformation changes from *trans* to *gauche*, through a combination of spectroscopies (FTIR and Raman) and X-Ray diffraction (WAXS). In parallel, through solid-state NMR, Ishii et al. [27,28] were the first to study the proton spin lattice relaxation time of these polymers to determine the mechanisms of the chain motion. They showed that, in the crystal, the chains experience a vigorous motion of *trans-gauche* conformational exchange above the crystal-crystal transition, which does not depend on the VDF content. Aimi et al. [29,30] also studied the mobility of these copolymers through solid-state NMR and measurements of the relaxation time in rotating frame $T_{1\rho}^{F}$, which can be associated with the chain mobility (molecular motion) involved in these polymers with frequencies in the kHz (or timescale of μs-ms) range. They evidenced that the *trans-gauche* exchange motion occurs at different temperatures upon the chemical sequences (e.g., VDF chain sequences and VDF-TrFE H–H linkage are activated at lower temperature than the VDF-TrFE H-T linkage). According to these authors [27–30], this mobility at high temperature induces the hexagonal symmetry of the PE phase. In the same way, the enhanced mobility of the dipole in the crystalline domains leads to the paraelectric behavior [25].

The descriptions of the transition made by Tashiro (*trans-gauche* exchanges leading to a conformational disorder) [9] and Aimi et al. or Ishii et al. (mobility of chemical sequences activated at different temperatures) [30,31] can also be understood with the thermodynamic formalism described by Wunderlich [17]. Indeed, the PE phase can be considered as a condis phase as indicated initially in 1988 [17] and recently recalled [32]. It is therefore interesting to merge these visions to improve the understanding of the transition to this high temperature two-dimensional hexagonal PE phase, which can be considered as a mesophase, i.e. an intermediary state between the solid crystal and the melt. From the low temperature copolymer crystal LT structure (FE or DFE), the transition activated with the motion of specific chemical sequences, would be more or less facilitated by the initial more or less dense crystalline structure, respectively FE or DFE. This relationship between chemical sequences mobility and crystalline phase densities can be assessed by associating temperature-dependent WAXS and solid-state NMR studies, which is the goal of this study.

In this article, two fluorinated copolymers with different VDF/TrFE compositions (46/54 and 65/35) were used and studied in the form of either solvent-cast, annealed, or annealed and polarized films. These compositions and specific treatments were chosen in order to select various crystal states: pure FE phase, mixed FE/DFE (or RFE) phases and pure DFE (or RFE) phase. From these various crystal phases, the transition to the condis crystal was examined by different techniques, such as differential scanning calorimetry (DSC), X-Ray diffraction at wide and small angle (WAXS-SAXS), solid-state NMR, and dielectric spectroscopy. These experimental techniques allowed for probing both the static (DSC, SAXS-WAXS) and dynamical behavior (solid-state NMR) of chains in the amorphous and in the crystalline phases to study the relationship between the chain mobility and the microstructure. To the best of our knowledge, these techniques have never been associated in a same study to understand the phase transition in fluorinated copolymers.

2. Experimental section

2.1. Materials and films preparation

P(VDF-*co*-TrFE) copolymers powders were provided by Piezotech (Arkema, France). Powders were dissolved in methylethylketone (MEK) at 14% by using a reflux set-up at 60 °C and 500 rpm agitation speed for 3 h, in order to obtain a homogeneous solution. Each solution was then filtered (0.6 μm), in order to remove every residual impurity. Films were made by bar coating: the polymer solution was spread onto a glass substrate, by using a bar coater. The solvent evaporation was performed

Table 1
Composition and annealing conditions for different film samples.

	Composition (mol %) VDF/TrFE	Drying conditions	Annealing conditions
Copo65-SC	65/35	30 min at RT	
Copo65-A	65/35	30 min at RT	1 h at 130 °C
Copo46-SC	46/54	30 min at RT	
Copo46-A	46/54	30 min at RT	1 h at 145 °C

at atmospheric pressure and room temperature (RT, ca. 20 °C) for 30 min. Solvent-cast films (20 μm thickness) were named Copo65-SC and Copo46-SC. Part of both films underwent an annealing step in oven, according to their respective composition. Each film was kept at T_m – 15 °C for 1 h and, then, cooled inside the oven until 70 °C to avoid thermal shocks. These annealed samples were named Copo65-A and Copo46-A. Information on various films and thermal treatments are gathered in Table 1.

2.2. Dielectric spectroscopy

Dielectric measurements were achieved on an Alpha-Analyzer (Novocontrol) spectrometer. Copo65-A and Copo46-A polymer films were placed between two circular titanium electrodes (1 cm diameter). A sinusoidal tension (1 V amplitude at 1-10^6 Hz) was applied to determine the complex relative permittivity ε (ε', ε'', and tan $\delta = \varepsilon''/\varepsilon'$). At the same time, temperature ramps at 3 °C/min were applied using a Quatro Cryosystem (Novocontrol). A first heating until T_m – 15 °C was performed to ensure a good thermal contact between the electrodes and the films. Data were recorded during the cooling back to 0 °C and upon the second heating up to T_m – 15 °C.

2.3. Polarization–electric field (P–E) loops

Films were placed between two gold electrodes and then the system was kept in compression (150 kN) thanks to a hydraulic press. Electrodes were connected to high-voltage amplifier and an ammeter. The poling process was performed on 1 cm^2 surfaces of Copo65-A and Copo46-A films (~20 μm thick) at room temperature. The charging–discharging electric field cycles were first applied to 25 V/μm followed by 25 V/μm steps until reaching 150 V/μm at 0.06 Hz frequency. After removing the resistive and capacitive contributions from the raw current, the current was integrated over time. This numerical treatment gave access to the P-E cycles and to their characteristic parameters: the remnant polarization (P_R), the spontaneous polarization (P_S), and the coercive field (E_C). The films recovered after this polarization experiment are named Copo65-A-Pol and Copo46-A-Pol.

2.4. SAXS-WAXS experiments

Simultaneous Small and Wide-Angle X-rays Scattering (SAXS and WAXS) experiments were performed on the Xenocs Nano-inXider SW system in transmission mode using Cu K_α radiation ($\lambda = 1.54$ Å) from an X-ray microsource (GeniX3D) operating at 50 kV-0.6 mA (30 W). Scattering patterns were collected using the combination of two detectors Pilatus3 (Dectris) operating simultaneously in SAXS and WAXS positions. The reduction of 2D datasets from the Pilatus3 detectors to 1D was achieved by radially averaging the raw data detector counts using Foxtrot data reduction software [33]. Distances between the sample and the SAXS and WAXS detectors are fixed allowing a continuous q range between q_{min} and 4.2 $Å^{-1}$, q_{min} is defined by the collimation used. q_{min} = 0.006 $Å^{-1}$ or 0.01 $Å^{-1}$ for collimation of 400 μm or 800 μm, the acquisition time was respectively set at 2400 s or 600 s for static experiments. Films were studied at room temperature as well as during thermal cycles up to the annealing temperature. For the in-situ thermal experiments, 20 μm thick films were put in between two aluminum foils in a Linkam hot stage (HFSX350) and submitted to thermal ramps (rate 10 °C/min) having plateaus every 5 °C to enable SAXS-WAXS data acquisitions. After stabilizing the temperature, the SAXS-WAXS patterns were recorded during 60 s (collimation 800 μm) at each defined temperature.

In-situ thermal experiments were also carried out on the SWING beamline at the Soleil synchrotron facility (project n°: 20210035). The X-Ray beam energy was set to 10 keV, leading to a wavelength of 1.24 Å. SAXS patterns were collected using an EigerX4M (Dectris) detector, positioned at 4.29 m from the sample, leading to a q range between 0.002 and 0.24 $Å^{-1}$. Data were acquired every 30 s, with an exposure time of 200 ms, during a thermal cycle at 10 °C/min using a Linkam THMS 600 heating stage, up to annealing temperature.

WAXS spectra, $I(2\theta)$ or $I(q)$, were fitted using the Fityk0.9.8 software [34] in the full 2θ (or q) range. With this software, each WAXS spectrum is decomposed into crystalline and amorphous contributions. The crystalline peaks are associated with sharp peaks while amorphous signal is fitted by broad peaks. The $2\theta_{hkl}$ (or q_{hkl}) of each crystalline peak gives the inter-planar distance d_{hkl} using Bragg's law:

$$2d_{hkl} \sin \theta_{hkl} = \lambda \text{ and } q_{hkl} = \frac{4\pi \sin \theta_{hkl}}{\lambda} = \frac{2\pi}{d_{hkl}} \quad (1)$$

A weight crystallinity χ_C of films was calculated using the following equation:

$$\chi_C = \frac{A_c}{A_c + A_a} \times 100\ [\%] \quad (2)$$

in which A_c and A_a are the areas under fitted crystalline peaks and amorphous halos, respectively.

From the raw SAXS data, a background subtraction is required before analyzing the SAXS spectra $I(q)$. For static experiments at room temperature, the background is a spectrum acquired without sample. For in-situ experiments, the background is a spectrum acquired with two aluminum foils in the Linkam heating stage. The Lorentz-corrected SAXS intensity profiles $q^2 I(q)$ were plotted and analyzed. For semi-crystalline polymers, the crystalline lamellae are periodically organized with the amorphous phase. The period of this organization is called long period, L_P. A correlation peak characterizing this periodic organization can be observed in $q^2 I(q)$ spectra. From the position of this peak, q_{max}, the averaged long period was determined using Equation (3):

$$L_P = \frac{2\pi}{q_{max}} \quad (3)$$

2.5. Differential scanning calorimetry (DSC)

DSC measurements were performed using a Q1000 series TA Instruments. Disks of polymer films were cut using a 6 mm cylindrical shape punch and superimposed in a DSC aluminum pan to reach 9-10 mg. Heating and cooling ramps were done at 10 °C/min under nitrogen flow (50 mL/min). Temperature ranges were adapted to each composition (from 0 °C to $T_{annealing}$).

2.6. Solid state nuclear magnetic resonance (NMR)

The copolymer films were analyzed on a Varian-600MHz spectrometer (Larmor frequency 600 MHz for ^1H, 564 MHz for ^{19}F). A 2.5 mm MAS (Magic Angle Spinning) probe HFXY was used with a spinning rate of 29 kHz and 3 μs τ_{90} pulse length was used for both ^{19}F NMR in Direct Polarization (DP or single pulse) pulse sequence. 2.5 mm zirconium rotors were used. Films were tightly rolled up and inserted into the rotors with an insert in Kel-F (PCTFE). The influence of Kel-F on ^{19}F spectra has been estimated at 0.1%. ^{19}F SSNMR spectra chemical shifts were referenced to $CFCl_3$ (0.0 ppm). A spectral width of 192 kHz was used to acquire the spectra with four scans for both nuclei. The temperature of the probe was regulated at 20 °C with a cooling unit and was measured above the stator. For $T_{1\rho}$ measurements, a Spin-Lock pulse sequence (Fig. SI–1) has been used with a B_1 RF-field strength of 83 kHz (τ_{90} = 3 μs). Series of 30 values of t_{lock} ranging from 0 to 30 ms with exponential increment, synchronized to the MAS rotation, were chosen. Offset value of −158 ppm in ^{19}F NMR spectrum was chosen in order to irradiate both CF_2 and CFH groups. A direct polarization spectrum (DP) was recorded to obtain quantitative spectra with a recycling delay of 10 s ensuring complete relaxation, a pulse duration τ_{90} = 3 μs and four transients. $T_{1\rho}$ measurements were also made at 50, 75, and 100 °C on heating and cooling process while DP spectra were recorded from 20 to

100 °C with a temperature step of 5 °C on heating and cooling. Deconvolution of spectra was performed for each DP and Spin-Lock spectra on DMFit software [35]. This software enables spectra to be reconstructed and considers baseline artifacts.

For $T_{1\rho}$ measurements, the intensities (Curve areas) of the different contributions are plotted as a function of t_{lock}. The magnetization $M_z(t_{lock})$ can be fitted by the following mono- or biexponential functions, shown in Equations (4) and (5), respectively:

$$M_z(t_{lock}) = \left[A.\, e^{-t_{lock}/T_{1\rho}}\right] (\text{Mono} - \exp) \quad (4)$$

$$M_z(t_{lock}) = \left[A_1.\, e^{-t_{lock}/T_{1\rho}'} + A_2.\, e^{-t_{lock}/T_{1\rho}''}\right] (\text{Bi} - \exp) \quad (5)$$

The different areas $M_z(t_{lock})$ of each contribution can be expressed as a function of t_{lock} depending on the relaxation times ($T_{1\rho}$, $T_{1\rho'}$, and $T_{1\rho''}$) in the rotating frame ($'$ and $''$ indicate short and long relaxation time respectively). A_1 and A_2 intensities of the signals are associated with the different relaxation times according to Equation (5). Ratios (%X_1 and %X_2) of each contribution can be estimated according to Equation (6):

$$\%X_1 = 100 \times \frac{A_1}{A_1 + A_2} \text{ and } \%X_2 = 100 \times \frac{A_2}{A_1 + A_2} \quad (6)$$

Fits with mono- or biexponential component using Origin software (Levenberg-Marquardt algorithm) were performed to obtain all $T_{1\rho}$, X_1, and X_2 values.

3. Results

The two P(VDF-*co*-TrFE) copolymers, Copo65 and Copo46, for which the transitions to the high temperature phase are studied have two significantly different VDF/(VDF + TrFE) ratios, respectively 65 and 46. Their room temperature macroscopic properties, for example the polarization, are very different, and can be significantly modified by heat treatment.

3.1. Applied macroscopic properties

3.1.1. Dielectric spectroscopy

Fig. 1 shows the dielectric spectroscopy responses ($\varepsilon' = f(T)$) of the two annealed copolymers during thermal cycles up to their respective annealing temperatures and carried out at different frequencies. Indeed, the evolution of the maximum of dielectric permittivity (ε'_{max}) as a function of frequency and temperature during cooling and heating serves as the key criterion for defining the material as ferroelectric or relaxor ferroelectric [36,37].

Fig. 1a shows the dielectric spectroscopy curves ($\varepsilon' = f(T)$) for Copo65-A. A maximum of dielectric permittivity is detected during both heating and cooling ramps, at 90 and 75 °C, respectively, showing a thermal hysteresis. The temperature of the maximum ($T(\varepsilon'_{max})$) is independent of the frequency used to perform the analysis. The thermal hysteresis and the independence of $T(\varepsilon'_{max})$ with respect to the frequency are associated with a ferroelectric behavior. Fig. 1b show the results of dielectric spectroscopy for Copo46-A. A maximum of dielectric permittivity is still detected, around 60-75 °C, on both ramps, but the signal is wider and its thermal hysteresis is low (ca. 5 °C). In addition, ε'_{max} shifts towards higher temperatures when the frequency varies from 1 kHz to 1 MHz. The increase of $T(\varepsilon'_{max})$ with frequencies associated with a relaxor ferroelectric behavior, even if the value of the dielectric constant, at room temperature, is small compared to the values usually reported for a relaxor ferroelectric material [37,38]. Moreover, although the thermal hysteresis is low, it is a sign of feeble ferroelectric behavior.

3.1.2. Bipolar polarization

Fig. 2 shows the polarization loops at 150 V/μm for both copolymers before and after annealing. Displacement−electric field (D−E) loops are given for information in supplementary materials (Fig. SI–2). For Copo65-SC and Copo46-SC, the effect of the composition translates into a thinner P-E cycle for the lower VDF content. The remnant polarization (P_R) and the coercive field (E_C) are significantly lower for Copo46-SC than for Copo65-SC (see Fig. 2 and Table 2). In both cases, the effect of the annealing performed in order to increase the crystallinity is clearly visible. For Copo65-A, the annealing treatment leads to a strong increase of the remnant polarization and spontaneous (P_S) polarization, as well as a slight decrease of the coercive field necessary for the dipoles switching.

The evolution of P_R and P_S after annealing is less pronounced for Copo46-A. On the other hand, a strong decrease of E_C is observed (Fig. 2b and Table 2). The high remnant polarization measured at room temperature in Copo46-A can be explained by the high temperature of the maximum of ε' (around 60 °C, Fig. 1b). Indeed, for a relaxor ferroelectric polymer, the remnant polarization and the coercive field increase when the temperature decreases [36]. The shape and the values of the P-E cycle for Copo65-A correspond to a ferroelectric behavior, while the P-E cycle for Copo46-A is characteristic of a relaxor ferroelectric behavior.

The different polarization cycles obtained for Copo65-SC, Copo65-A, Copo46-SC, and Copo46-A reflect, among other things, their different crystalline organizations. Conversely, the polarization can induce a change in the crystalline organization. To study this impact, the annealed films polarized during the bipolar polarization experiment were collected, named Copo65-A-Pol and Copo46-A-Pol and analyzed

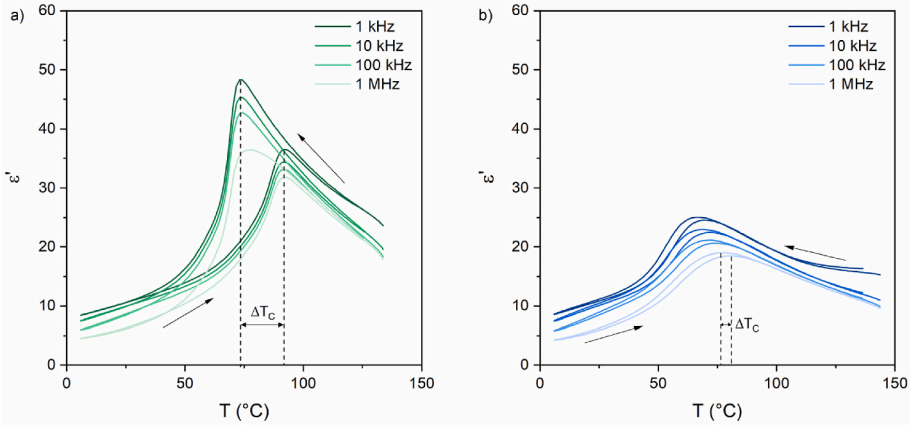

Fig. 1. Dielectric spectroscopy experiments on annealed copolymer films; evolution of the dielectric constant with the temperature (arrows indicate the heating and cooling temperature variations) for the two amounts of TrFE and for various frequencies, from 1 kHz to 1 MHz. (a) Copo65-A and (b) Copo46-A.

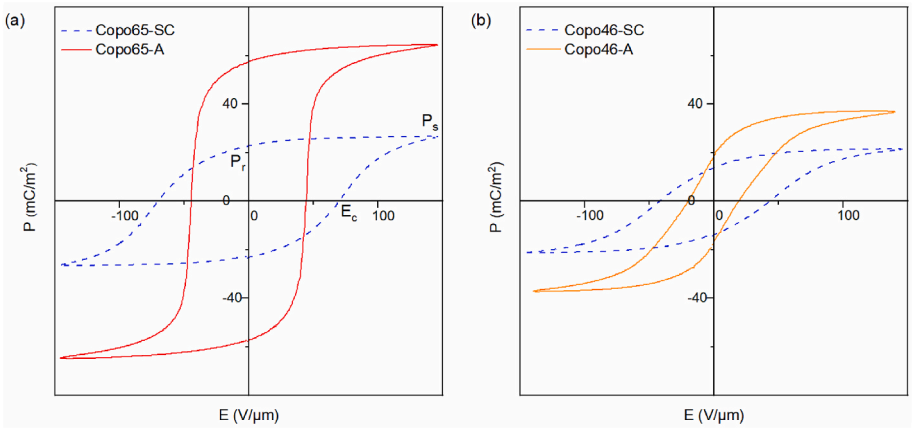

Fig. 2. Bipolar P-E loops of solvent cast (dash line) and annealed (solid line) films: (a) Copo65-SC and Copo65-A and (b) Copo46-SC and Copo46-A.

Table 2
Remnant and saturated polarizations and coercive field of solvent-cast and annealed film for different copolymer samples.

	P_R (mC/m^2)	P_S (mC/m^2)	E_C (V/μm)
Copo65-SC	23	26.5	70
Copo65-A	58	64	44
Copo46-SC	14	37	44
Copo46-A	19	44	19

along with the solvent-cast and annealed samples.

3.2. Crystalline structure and morphology

3.2.1. SAXS-WAXS

Fig. 3 combines WAXS and SAXS spectra for the two copolymers which underwent the different treatments: solvent-casting (-SC), annealing (-A), and annealing and polarization (-A-Pol).

Fig. 3a and b provide the comparison of the crystalline structure according to the chemical composition of the copolymer (Fig. 3a for VDF/TrFE = 65/35 and Fig. 3b for VDF/TrFE = 46/54), and according to the thermal and polarization treatments.

The WAXS spectra for Copo65-SC, Copo65-A, and Copo65-A-Pol show at least three crystalline peaks. The main crystalline peak at ca. 1.4 Å^{-1} corresponds to the juxtaposition of the (200) and (110) peaks, which are characteristic of the crystalline order perpendicular to the chains ($d_{200/110} \sim 4.55$ Å) [10]. The other two peaks between 2.25 Å^{-1} and 3.0 Å^{-1} are the juxtaposition of various Bragg peaks which are related to the inter- and intra-chain order, in particular the first peak, which contains the (001) peak [10]. All these peaks are associated with the coexistence of FE and DFE phases, as already described in the literature [10]. The annealing and the polarization are responsible for an increase of crystallinity (from 18 to 33%), as well as for the evolution of the fractions of the crystalline phases. The quantification of these phases, deduced from the peak-fitting of Bragg peaks (Fig. SI–3) has already been detailed elsewhere [39]. The quantitative results are summarized in Table 3. The annealing step leads to an increase of the crystallinity and of the fraction of the DFE defective phase. The polarization of the annealed film induces a sharpening of the diffraction peaks, which is interpreted by the transition of the DFE phase towards the FE phase

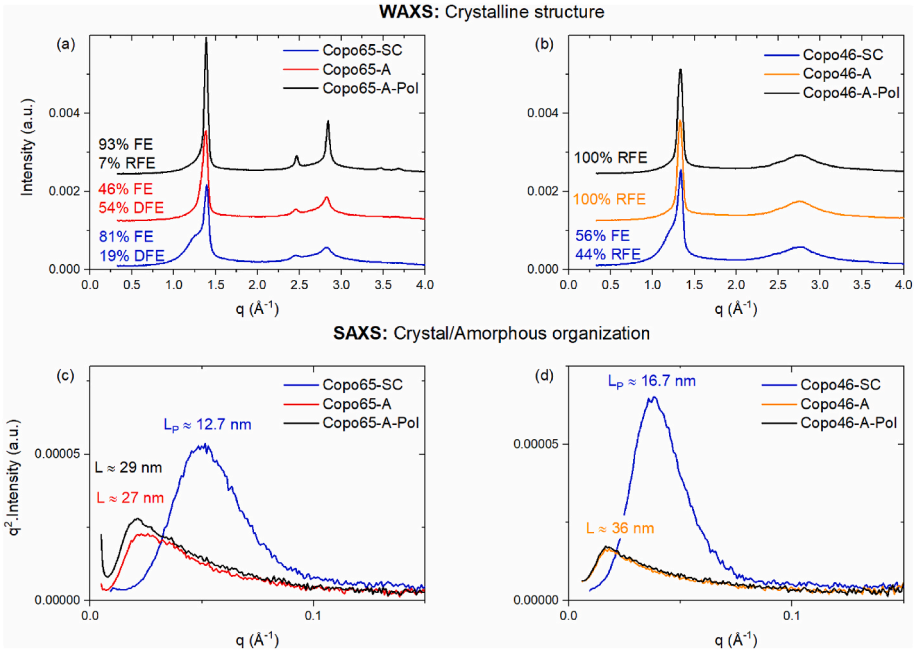

Fig. 3. (a)-(b): WAXS and (c)-(d): SAXS spectra for the two P(VDF-*co*-TrFE) compositions. (a)-(c): Copo65 and (b)-(d): Copo46. The various preparation conditions are compared: solvent cast (-SC), annealed (-A), and annealed-polarized (-A-Pol).

Table 3
Overall crystallinity and respective fractions of FE, DFE, and RFE phases for all the samples.

Sample name	χ_C from WAXS (%)	FE fraction (%)	DFE or RFE fraction (%)
Copo65-SC	18	81	19
Copo65-A	**30**	**46**	**54**
Copo65-A-Pol	**34**	**93**	**7**
Copo46-SC	14	56	44
Copo46-A	**22**	**0**	**100**
Copo46-A-Pol	22	0	100

under an electric field. It is recalled that the difference between the two defective phases (DFE and RFE) is that the DFE is polarizable and can be transformed into FE, while the RFE phase is not polarizable. After polarization, the peaks associated with the defective phase almost disappear (Fig. SI–3). The remaining fraction (7%) is therefore not polarizable and consequently called RFE. The hypothesis to explain these different behaviors could be the existence of a critical $d_{200/110}$ inter-planar distance around 4.70–4.75 Å, at 25 °C, which separates the DFE and RFE phases [39].

The WAXS spectra for Copo46-SC, Copo46-A, and Copo46-A-Pol almost show a unique crystalline peak at ca. 1.3 $Å^{-1}$ (Fig. SI–4). The Bragg peaks between 2.25 $Å^{-1}$ and 3.0 $Å^{-1}$ have almost disappeared. This means that the order within the polymer chains (intra-chain order) is disrupted by the incorporation of a large amount of TrFE. For Copo46-SC, the increase of the TrFE content in the chains leads to an expansion of the crystalline lattice ($d_{200/110} \sim 4.7$ Å), which is related to the incorporation of TrFE motif into the crystal. Moreover, the fraction of RFE phase is higher than for Copo65-SC, and the overall crystallinity is slightly lower (Table 3). The annealing treatment induces both an increase of crystallinity (from 14 to 22%) and the conversion of the FE phase into the defective one. Since the WAXS spectra before and after polarization are superimposable, the existing defective phase is not polarizable and can be qualified as RFE.

Fig. 3c and d shows the SAXS spectra at room temperature for the two copolymers before and after annealing and after polarization. For Copo65-SC and Copo46-SC, a correlation peak can be observed. The maximum corresponds to the long period (L_P), i.e. the sum of the thickness of a crystalline lamella (L_c) and of a layer of amorphous phase (L_a). The long periods are 13 nm and 17 nm for Copo65-SC and Copo46-SC, respectively. The increase of L_P when the TrFE content increases may reflect the thickening of the crystalline lamella. This higher value for L_c can be explained by the increasing rigidity of the polymer chains, which hinders the folding. For comparison, the long period of a poly(trifluoroethylene) (PTrFE) sample with a similar thermal treatment was measured. Its value is 21 nm (Fig. SI–5) and it confirms that L_P increases with the TrFE content.

After annealing, the correlation peak significantly shifts towards lower q values. This evolution is related to the existence of a superstructure peak, which is associated with the appearance of semi-crystalline domains made of stacks of crystalline lamellae and amorphous phase. A detailed description of these objects observed by AFM and SAXS has recently been published [40]. The characteristic dimensions of these semi-crystalline domains are ca. 27 nm and 36 nm for Copo65-A and Copo46-A, respectively. The polarization induces a slight evolution of this SAXS signal only for Copo65-A-Pol: the signal is more intense and the peak is shifted towards lower q values.

The higher P_R and P_S values for Copo65-A compared to Copo65-SC can be attributed to the significant increase in the fraction of the polarizable crystalline phase (DFE), which is induced by the annealing treatment. A previous study on P(VDF-*ter*-TrFE-*ter*-CTFE) terpolymers showed that the evolution of P_R was well correlated with the evolution of the polarizable crystalline phases (FE + DFE) [39]. The increase in the remnant and the spontaneous polarizations after annealing is much less important for Copo46-SC. For Copo46-A, the P_R value would not be linked to the fraction of the polarizable phases (FE or DFE), since these phases disappear after annealing. This value would be associated with the high $T(\varepsilon'_{max})$ (compared to room temperature), as mentioned previously and reported in the literature [36]. The slight increase of P_R after annealing is related to the increase of crystallinity.

It can be concluded that an annealing treatment performed at T_m - 15 °C during 1 h significantly increases the crystallinity and the defective phase fraction. The polarization leads to the transformation of DFE phase into FE phase, but does not affect the RFE phase. WAXS analyses enabled the identification and selection of three samples with strongly different crystalline nature, which should exhibit different behaviors during in-situ temperature-dependent measurements up to the condis phase. Copo65-A-Pol contains almost only the FE phase and 34% of overall crystalline fraction. Copo46-A only contains RFE defective phase, with an overall crystallinity of 22%. In the end, Copo65-A (χ_C = 30%) has a 50/50 ratio of FE and DFE phases.

3.2.2. *Solid-state NMR*

To gain a better understanding of the crystalline phases, we studied the same P(VDF-*co*-TrFE) copolymers by solid-state NMR (SS-NMR). Here, we examine the molecular dynamics through relaxation times $T_{1\rho}$ as functions of temperature for films of P(VDF-*co*-TrFE) copolymers.

Our methodology consists in analyzing the SS-NMR spectra and the relaxation times at room temperature (20 °C) and at high temperature (100 °C), to identify the characteristic signals of the amorphous and crystalline phases present in the polymer films. SS-NMR spectra were assigned according to the work of Mabboux et al. [41] in HR-NMR. A direct comparison of the ^{19}F HR- (Fig. 4c) and SS- (Fig. 4a and b) spectra at 20 °C is shown in Fig. 4.

Fig. 4 clearly shows that the SS-NMR spectrum of Copo65-A at 100 °C is very similar to the HR spectrum of this copolymer. Although the resonances are much broader, the chemical shifts shown in the SS-NMR spectrum at 100 °C (Fig. 4b) are almost identical to those observed in the HR-NMR spectrum (Fig. 4c). These observations indicate that at high temperature the ^{19}F spin dynamics is fast enough for the NMR signal to be averaged almost as in the liquid state. A total of 14 peaks is observed at 100 °C and these peaks are also present at room temperature with broader widths. The SS-NMR spectrum of Copo65-A at 20 °C (Fig. 4a) possesses additional signals which do not correspond to any resonances

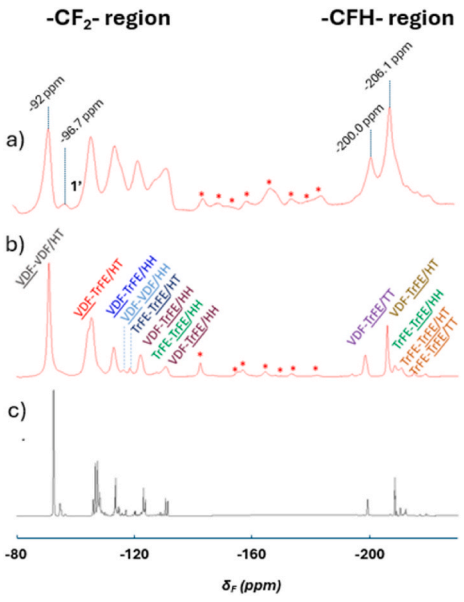

Fig. 4. ^{19}F 564 MHz SS-NMR DP in MAS at 29 kHz spectra of Copo65-A a) at 20 °C; b) at 100 °C and c) ^{19}F 376 MHz HR-NMR spectrum of Copo65 in acetone-d_6 at 25 °C. Label 1′ designates the peak at −96.7 ppm. * in the MAS SS-NMR spectra indicate spinning sidebands.

present in the HR-NMR spectrum. For example, the peak at −96.7 ppm (peak 1′ on Fig. 4a) is located between two types of CF_2 associated with sequences VDF-VDF/H-T and VDF-TrFE/H-T. According to previous reports on the microstructure of PVDF and P(VDF-*co*-TrFE) [29,30,41–45], this peak at −96.7 ppm is associated with CF_2 of VDF-VDF/HT in all-*trans* conformation highlighting the polar and likely ferroelectric behavior of this polymer. It corresponds to the all-*trans* conformation of the VDF-VDF/H-T sequence, according to previous studies dedicated to α-PVDF and β-PVDF [43]. Wormald et al. indeed identified one chemical shift for fluorine *gauche* (ca. −82 ppm) and another one for fluorine *trans* (ca. −96.7 ppm) and in between, the peak of exchange between the two conformations [43]. The presence of these conformations peaks is highlighted by $T_{1\rho}^{F}$ measurements with long spin lock experiments (t_{lock} = 30 ms). The deconvolution of this long spin lock spectrum is displayed in Fig. 5, details on the deconvolution are presented in SI.

Thanks to this deconvolution, six new peaks were found. As they are not observed in the HR spectra, these new peaks likely correspond to CF_2 or CFH motifs associated with ^{19}F spins locked in specific conformations endowed with slow spin dynamics. These signals were thus assigned to fluorinated motifs of the crystalline phases, as already reported in the literature [42], especially the studies by Aimi et al. [29,30]. They identified peaks 1′, 9′, and 10′ and associated these peaks with the crystalline all-*trans* conformation peaks 1 (VDF-VDF/HT junction), 9 (VDF-TrFE-VDF/TT-HH junction), and 10 (VDF-TrFE/HT junction), respectively [29]. According to their chemical shifts, peaks 9′ and 10′ most probably correspond to the VDF-TrFE-VDF/TT-HH and VDF-TrFE/HT sequences. The additional contributions (peaks 2′, 3′, and 4′) behave similarly, and were assigned, by analogy with Ando's work [42]. Peak 2′ can either be associated with VDF-VDF/HT or VDF-TrFE/HT because of its proximity to peaks 1 and 2. It thus corresponds either to VDF-VDF/HT (peak 1) and a slightly different all-*trans* conformation to that observed for peak 1′ or to VDF-TrFE/HT junction (peak 2) and a fluorine-*gauche* conformations. Peaks 3′ and 4′ are associated with a VDF-TrFE junction. We can make the hypothesis that peak 3′ is associated with VDF-TrFE/HT (peak 3) and peak 4′ with VDF-TrFE/HH (peak 4) because these conformation peaks are also

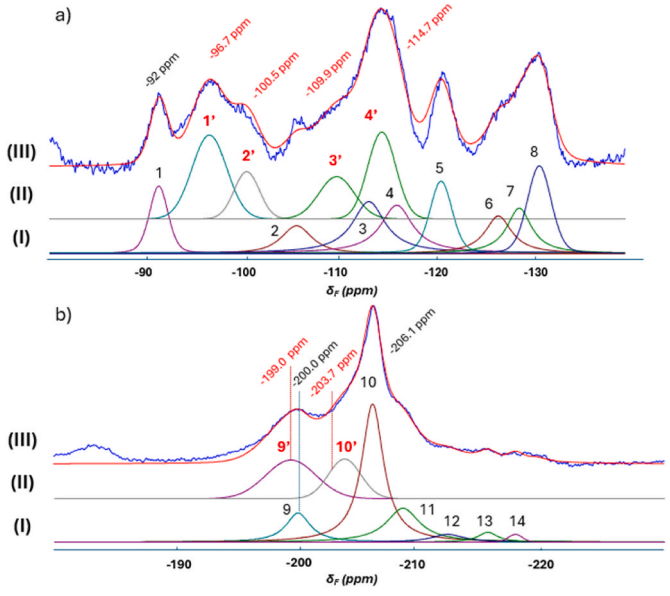

Fig. 5. Copo65-A, deconvolution of ^{19}F SL experiment at 20 °C with t_{lock} = 30 ms in a) CF_2 region and b) CFH region. For each region: (I) shows contributions derived from the 100 °C DP spectrum (peaks 1-14), (II) displays additional contributions observed at t_{lock} = 30 ms (peaks 1′-10′), and the spectra (III) are the experimental (blue) and simulated (red) spectra. (For interpretation of the references to colour in this figure legend, the reader is referred to the Web version of this article.)

observed in the CFH region with peaks 9′ and 10′. In the future section, the peaks 1′, 9′, and 10′ will be discussed to compare with Ando's work [42].

To better highlight the behavior of these peaks, $T_{1\rho}^{F}$ relaxation times were measured thanks to the evolution of peak intensity as function of t_{lock} displayed in Fig. 6 [42]. $T_{1\rho}^{F}$ were measured for all the deconvoluted signals. The $T_{1\rho}^{F}$ of peaks 1, 9, and 10 are isolated in Fig. 6a, and of peaks 1′, 2′, 3′, 4′, 9′ and 10′ are shown in Fig. 6b and Table 4 exhibits all the values of $T_{1\rho}^{F}$.

Fig. 6a shows that the evolution of intensity of peak 1, 9, and 10 vs t_{lock} can be fitted with a biexponential function revealing two $T_{1\rho}^{F}$, a short one and a long one (see Equations (5) and (6) and Table 4). This biexponential behavior, observed with or without ^{1}H decoupling, can be explained by the presence of two phases with different relaxation regimes (a fast one and a slow one). In contrast, the behavior of intensities of peaks 1′ to 10′ (Fig. 6b) can be fitted with a mono-exponential function corresponding to only one $T_{1\rho}^{F}$ (for each signal) much longer than those determined for peak 1, 9, and 10. These long $T_{1\rho}^{F}$ indicate slow relaxation regime caused by low mobility and thus corresponds to spins located in crystalline phases. Fluorinated motifs associated with these long $T_{1\rho}^{F}$ are thus likely located in the FE phase [42,45,46].

For each peak (1, 9, and 10), a biexponential model is observed and are in agreement with Aimi [29]. However, in their study, the height of peak was used and two explanations are given for the biexponential components: (1) the height of peaks is affected because of the presence of overlapping contributions (i.e. peak 1 at −91.9 ppm and peak 1′ at −96.7 ppm), (2) the spin diffusion from amorphous to crystalline phase. Since we performed deconvolution, the first explanation is no longer relevant, we can say that the two components of peaks 1, 9, and 10 corresponds to the amorphous phase and the spin diffusion.

Regarding the effect of the polarization on the relaxation time of Copo65-A: the values of $T_{1\rho}^{F}$ appear to be longer on all the contributions indicating a lower mobility on this sample, the dynamics is less efficient on Copo65-A-Pol. However, looking into WAXS results (Table 3), this difference should be much higher since after polarization the ratio FE/DFE doubled (from 46/54 in Copo65-A to 93/7 in Copo65-A-Pol). This means that it is not possible to distinguish the FE and DFE crystalline phases with SS-NMR since no major difference is observed between Copo65-A and Copo65-A-Pol. The long $T_{1\rho}^{F}$ contributions (peak 1′-10′ in Fig. 5) reflect the FE and DFE phases.

Copo46-A displayed a very different behavior with temperature, the number of peaks required to index the spectra at 20 and 100 °C is the same (Fig. SI–6). The peaks 1′-10′ observed in Copo65-A are not present in Copo46-A, indicating significant difference in the crystalline phases of the two copolymers (see Table 4). The analysis of intensity evolution of peaks as a function of t_{lock} for Copo46-A reported in Fig. SI–7 shows that all the contributions have similar short $T_{1\rho}^{F}$, even the contributions showing a biexponential behavior and thus two $T_{1\rho}^{F}$ (Table 4). These relaxation times (short $T_{1\rho}{}^{F}$ = 0.3-2.2 ms and long $T_{1\rho'}{}^{F}$ = 3.0-7.5 ms) are shorter than those of Copo65-A. In Copo46-A, all relaxation times are short, indicating a higher mobility similar to what is usually observed in amorphous phases. The signals (Fig. SI–7) shows no more signals after 7.5 ms of spin-lock while for Copo65, the magnetization is conserved for longer spin-lock time. However, according to the SAXS-WAXS study, two phases are observed in this copolymer: the RFE crystalline phase and the amorphous phase (Table 3). NMR results (Table 4) indicate that the crystalline phase RFE is quite mobile with $T_{1\rho}^{F}$ values close to that of the amorphous phase.

Copo65 shows six peaks associated with conformations (peaks 1′-10′) and long $T_{1\rho}$ relaxation time. In contrast, peaks 1, 9, and 10 feature shorter $T_{1\rho}$ relaxation times and the evolution of their intensities as a function of t_{lock} can be fitted with a biexponential model. This observation may be caused by the presence of two phases, an amorphous phase and another phase with a slower relaxation regime, or by spin diffusion. An important point to note is that conformational contributions are associated with VDF-VDF or VDF-TrFE junctions, none are

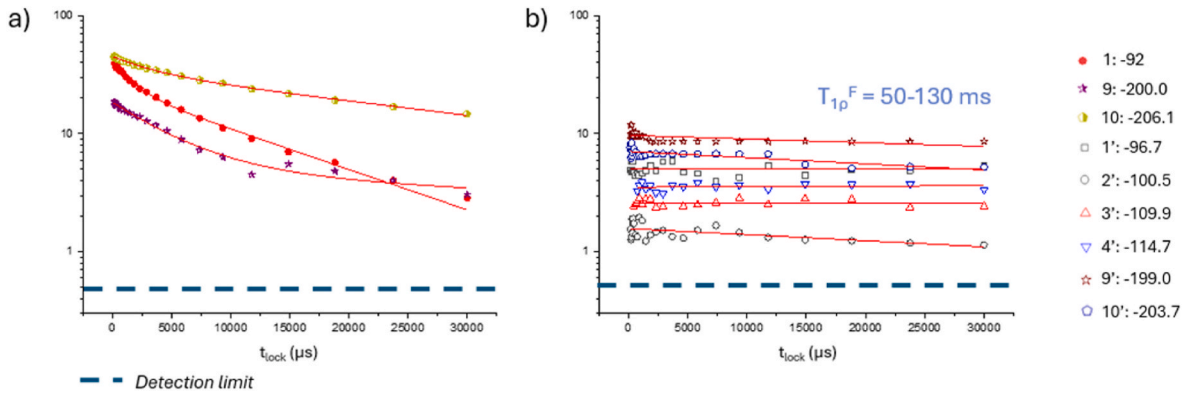

Fig. 6. Copo65-A, a) Evolution of intensity of peak 1, 9, and 10 as function of t_{lock} and b) Evolution of intensities of peaks 1′, 2′, 3′, 4′, 9′, and 10′ as function of t_{lock} at 20 °C. All symbols are associated with a chemical shift in ppm. The dashed blue line indicates the detection limit of the instrument. (For interpretation of the references to colour in this figure legend, the reader is referred to the Web version of this article.)

associated with TrFE-TrFE junctions.

For Copo46, only peaks 1, 9, and 10 are present and the evolution of their intensities as a function of t_{lock} can also be fitted with a biexponential model. In this case, the two components can be interpreted as contributions from the amorphous and RFE phases. No peaks from conformations are detected, indicating a more mobile system ($T_{1\rho}^{Copo46} < T_{1\rho}^{Copo65}$).

3.3. Evolution of properties during a thermal cycle

In order to study the « crystal to condis-crystal transition», different experiments during thermal ramps were carried out on the three selected samples. The objective is to highlight their different behaviors in the vicinity of the Curie transition.

3.3.1. DSC experiments

Fig. 7 shows the thermograms for the first heating until the annealing temperature, followed by the cooling down to 0 °C, for Copo65-A-Pol, Copo65-A, and Copo46-A.

In Fig. 7a, the thermograms for Copo65-A-Pol and Copo65-A are presented in black and red, respectively. The comparison of these plots shows that the polarization done at room temperature sharpens and shifts the Curie endothermal peak towards higher temperatures. This evolution is associated with the suppression of the DFE phase in favor of the FE phase, as well as with the perfection of the FE phase under polarization. The perfect superimposition of cooling thermograms, after heating up to the annealing temperature in the high temperature crystalline phase, shows that the effect of polarization is erased by this heating ramp. These observations have already been reported in the literature [10]. During the cooling ramp, the exothermal Curie peak common to both samples is detected at 66 °C. The thermal hysteresis (ΔT_C) observed for the Curie transition is 30 °C for Copo65-A-Pol and 21 °C for Copo65-A. This hysteresis is related to the first order behavior of the Curie transition and is consequently more important for Copo65-A-Pol than for Copo65-A. For Copo46-A (Fig. 7b), the enthalpic peaks associated with the Curie transition are not detected, only a wide signal is observed between 40 and 70 °C during both heating and cooling, with a thermal hysteresis of ca. 5 °C.

3.3.2. In-situ SAXS-WAXS experiments

In-situ SAXS and WAXS experiments were carried out for Copo65-A-Pol, Copo65-A, and Copo46-A during thermal ramps up to their annealing temperature. WAXS spectra were analyzed as already described in our previous studies [47], in order to plot the evolution of the inter-planar distances and of the crystallinity with respect to the temperature (Fig. 8). The decomposition of the spectra, performed in order to get quantitative information, is reported in Fig. SI–3 and SI-4 for three different samples.

Fig. 8a, b, and 8c show the evolution of inter-planar distances for Copo65-A-Pol, Copo65-A, and Copo46-A. The inter-planar distance at ca. 4.55 Å is associated with the FE phase. This phase is the majority phase for Copo65-A-Pol, while it represents 46% of the crystalline fraction of Copo65-A and is absent for Copo46-A (see Table 3). The intensity of the FE Bragg peak decreases when the temperature increases, while its position has only a slight evolution before the FE peak disappears completely at the end of the Curie transition (Fig. 8a and b). The other inter-planar distance below the Curie transition (Fig. 8a, b, and 8c) is associated with the defective crystalline phase. This distance increases continuously with temperature. At high temperature, only the paraelectric (PE) phase exists for the three samples (green symbols). This crystalline phase, different from the previous two, is characterized by a hexagonal crystalline lattice and by larger inter-planar distances, as well as by a dynamic conformational disorder [15]. The grey areas in Fig. 8a–b highlight the temperature ranges of the Curie transition during the heating ($T_{C\text{-heat}}$) and cooling ($T_{C\text{-cool}}$) ramps. In these ranges, the ferroelectric, defective, and paraelectric phases coexist. For this reason, grey symbols are used when the defective and paraelectric contributions are undistinguishable.

For Copo65-A-Pol, during the first heating (small orange circle symbols), the low fraction (7%, see Table 3) of defective phase corresponds to the non-polarizable RFE phase, since the polarization step transforms the DFE into the FE phase. The inter-planar distance of the RFE phase increases continuously above 50 °C (orange circles). Between 70 and 90 °C (grey circles) the RFE phase is undiscernible from the PE one, because their characteristic peaks are too close. In this temperature range, the Curie transition takes place. Starting from 100 °C, only the PE phase (green circles) is detected, and its lattice keeps expanding with the temperature. At the beginning of the cooling ramp, the PE phase (green crosses) is detected and its lattice parameters decrease continuously. The beginning of the Curie transition occurs at 65 °C, with the reappearance of the FE crystalline phase. Again, in the temperature range of the Curie transition (from 65 to 50 °C during the cooling ramp), the PE and the defective phase are undistinguishable. At the end of the cooling, the fraction of the defective phase is 35%, and can be considered as a mostly polarizable defective phase (DFE). Fig. 8a' shows the evolution of the crystallinity of Copo65-A-Pol with temperature. During the heating ramp, the crystallinity progressively decreases between 0 and 90 °C and then drops at the Curie transition. At the beginning of the cooling ramp, the crystallinity has a slight evolution and, at 70 °C, it steeply increases to finally reach a plateau. The initial crystallinity, which was obtained after polarization, cannot be retrieved after this thermal cycle. This observation is consistent with the results reported in Table 3 and shows that the DFE phase is less “crystalline” than the FE phase, because of the loss of order within the polymer chain (intra-chain order). The evolution

Table 4
Assignments of the signals observed in the deconvoluted SS-NMR spectra of the P(VDF-*co*-TrFE) copolymers to the fluorinated motifs and to their $T_{1\rho}^{F}$ (10^{-3} ms) (%X_1 and %X_2 in brackets).

Fluorine region	CF_2										CFH									
Peak number/δ_F (ppm)	**1/-92.0**	**1'/-96.7**	**2/-100.5**	**2/-106.2**	**3'/-109.9**	**3/-113.9**	**4'/-114.7**	**4/-116.5**	**5/-121.6**	**6/-123.2**	**7/-127.2**	**8/-129.2**	**11/-131.4**	**12/-194.8**	**9'/-199.0**	**9/-200.0**	**10'/-203.7**	**10/-206.1**	**13/-208.6**	**14/-212.6**	**15/-215.5**	**16/-217.8**	**17/-219.4**
Copo65-A	1.7 (46)	123	88 (100)	1.0 (46)	74 (100)	0.9 (46)	62 (100)	0.5 (51)	20.8	0.6 (49)	33.4 (100)	0.4 (40)	26 (100)	6.3	140 (100)	4.6 (65)	83 (100)	3.7 (27)	1.7 (37)	7.3	18.4	21.6	10.1
	12.3	(100)		8.4 (54)		13.5		33.5	(100)	8.7 (51)		36.0 (60)		(100)		45.9 (35)		35.8	27.8	(100)	(100)	(100)	(100)
	(54)					(54)		(49)										(73)	(63)				
Copo65-A-P	1.4 (53)	127	97 (100)	0.9 (54)	78 (100)	1.1 (41)	65 (100)	0.9 (37)	12.7	0.4 (53)	49 (100)[a]	27 (100)[a]	13.4 (100)	4 (100)	151 (100)	2.8 (39)	98 (100)	25.8	1.9 (39)	8.1	19 (100)	21.5	8.3
	18.9	(100)		9.8 (46)		12.1		20.3	(100)	7.9 (47)						22.2 (61)		(100)[a]	33.3	(100)		(100)	(100)
	(47)					(59)		(63)											(61)				
Copo46-A	0.3 (18)			0.4 (17)		0.6 (26)		1.2	4.1	0.9 (30)	2.8 (100)	3.1 (100)	4.3 (100)	0.5		2.2 (31)		2.4 (22)	1.4 (16)	1.2 (18)	2.9	5 (100)	4.2
	3.5 (82)			3.0 (83)		3.3 (74)		(100)	(100)	4.3 (70)				(100)		5.8 (69)		7.5 (78)	6.3 (84)	6.2 (82)	(100)		(100)
Associated sequence[b]	VDF-VDF/HT	VDF-VDF/HT	VDF-VDF/HT or VDF-TrFE/HT[c]	VDF-TrFE/HT	VDF-TrFE/HT[c]	VDF-TrFE/HH	VDF-TrFE/HH[c]	VDF-VDF/HH	TrFE-TrFE/HT	VDF-TrFE-VDF/HH-TT	TrFE-TrFE-VDF/HT-HH	TrFE-TrFE/HH	VDF-TrFE-VDF/HH-TT	VDF-TrFE/TT	VDF-TrFE-VDF/HH-TT	VDF-TrFE-VDF/HH-TT	VDF-TrFE/HT	VDF-TrFE/HT	TrFE-VDF/HH	TrFE-TrFE/HT	TrFE-TrFE/HH	TrFE-TrFE/TT	TrFE-TrFE/TT

[a] Not possible to fit with biexponential model.
[b] Fluorine concerned are underlined.
[c] Hypothesized sequence association.

of the crystallinity shows a thermal hysteresis of ca. 30 °C, associated with the disappearance and the reappearance of the FE phase during heating and cooling, respectively. This behavior is illustrated more in detail in the WAXS spectra reported Fig. SI–8. During the heating ramp, just below the Curie transition (Fig. SI–8a), the WAXS spectrum of Copo65-A-Pol exhibits four crystalline peaks. The weak contribution at $q = 1.32$ Å^{-1} is associated with the fraction of non-polarizable RFE phase, whereas the intense peak at $q = 1.38$ Å^{-1} corresponds to the juxtaposition of diffraction from the (110) and (200) planes of the FE phase. Similarly, the crystalline peak located at

$q = 2.5$ Å^{-1} arises from the juxtaposition of diffraction from (001), (310) and (020) planes and the last one at $q = 2.85$ Å^{-1} results from the juxtaposition of diffraction from (111), (201), (400) and (220) planes. The first Bragg peaks ($q \sim 1.3$-1.4 Å^{-1}) are characteristic of the inter-chains order, perpendicular to the chain axis, while the two other peaks at higher q mostly represent the order along the chains (intra-chain order). Just above the Curie transition (Fig. SI–8b), only the contribution of the PE phase ($q = 1.28$ Å^{-1}) is detected and the crystalline peaks at high q disappeared. Figure SI-8c and 8d show that this behavior is reversible during the cooling ramp. The disappearance/reappearance of the crystalline peaks located at high q, characteristic of the intra-chain order, as well as the disappearance/reappearance of the FE phase, are responsible for the steep variations of crystallinity in the vicinity of the Curie transition.

In the case of Copo65-A (Fig. 8b and b'), the 46% fraction of defective phase is mostly polarizable and, thus, can be qualified as DFE (red circle symbols in Fig. 8b). The inter-planar distance of the DFE phase slightly increases up to 40 °C, then its contribution is undistinguishable from that of the PE phase (Curie transition occurring between 50 and 85 °C). Above the Curie transition, only the PE phase exists and its lattice continues to expand until the annealing temperature. While cooling, the inter-planar distance of the PE phase (green crosses) first decreases reversibly. The Curie transition during the cooling ramp is detected between 60 and 40 °C. In this temperature range, the FE phase reappears and the PE phase is progressively transformed into DFE. Similarly, the crystallinity of Copo65-A (Fig. 8b') exhibits a drop during heating and a steep increase during cooling, which correspond to the disappearance and the reappearance of the FE phase, respectively. The same explanation as for Copo65-A-Pol concerning the crystallinity changes in the vicinity of the Curie transition (Fig. SI–8) works for Copo65-A. The thermal hysteresis for crystallinity is ca. 15-20 °C for Copo65-A, which is lower than the one measured for Copo65-A-Pol. For Copo65-A, it might be expected that the inter-planar distances and crystalline values are the same before and after the thermal cycle. The small discrepancy may be attributed to the different cooling rates experienced by the samples from the annealing temperature. Specifically, to prepare Copo65-A, the sample was cooled in an oven, compared to the controlled cooling rate applied during the in-situ experiment.

For Copo46-A (Fig. 8c), only one crystalline peak, which is associated with the RFE phase, is observed. This phase undergoes a continuous evolution towards the paraelectric phase, reversible without hysteresis at cooling. The evolution of crystallinity is also continuous, reversible, and without hysteresis (Fig. 8c').

For the three films, the thermal evolutions of the crystalline phases are coherent with the DSC thermograms showed in Fig. 7, in terms of temperature and hysteresis. The hysteresis is associated with the Curie transition, corresponding to the disappearance and reappearance of the FE phase (loss and recovery of the intra-chain order), upon heating and cooling, respectively. This order is absent in the RFE phase and, consequently, in Copo46-A.

During the same thermal cycles, the SAXS signals, which characterize the organization of crystalline lamellae, were followed. These experiences were performed with the Nano-inXider for Copo65-A-Pol and Copo65-A and at Soleil Synchrotron for Copo46-A. The 3D representations are shown in Fig. 9.

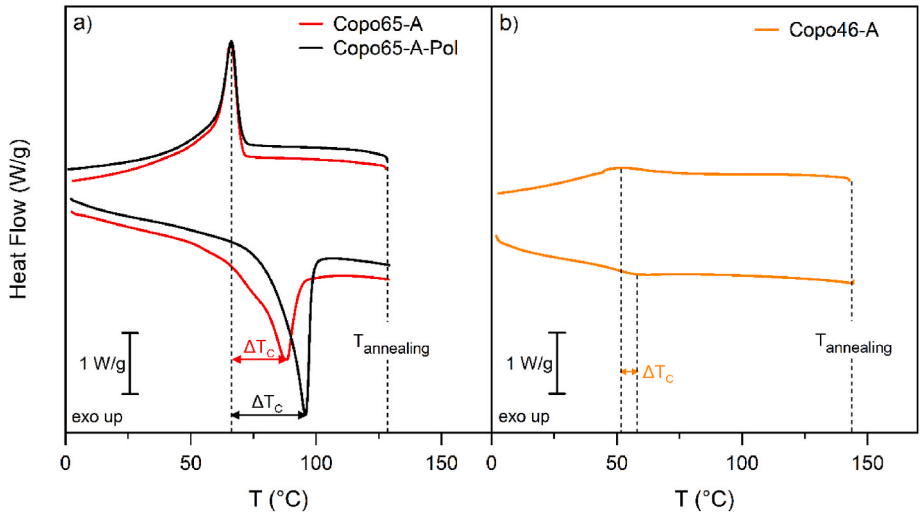

Fig. 7. DSC experiments on a) Copo65-A and Copo65-A-Pol and b) Copo46-A.

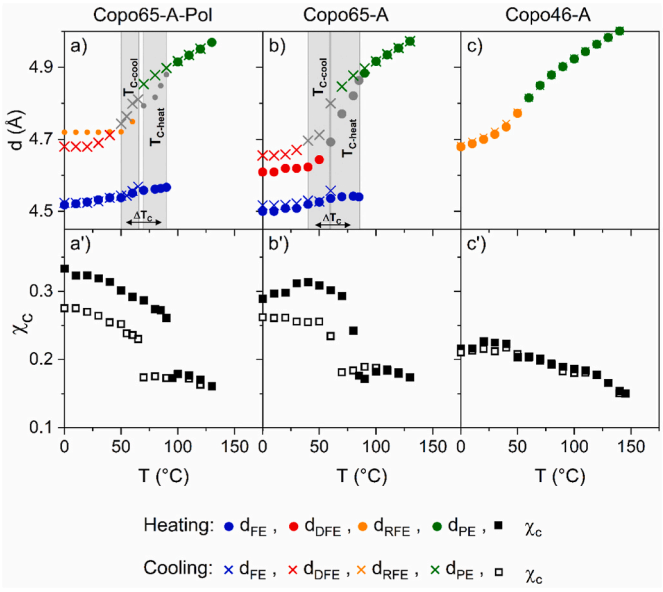

Fig. 8. Evolution of the inter-planar distances (a, b, and c) and the crystallinity (a', b', and c') with temperature. Smaller symbols in a) refer to a very low fraction of the RFE crystalline phase.

These evolutions clearly highlight a sharp transition for both Copo65-A-Pol and Copo65-A, during both heating and cooling ramps, and a continuous evolution for Copo46-A. This SAXS signal reflects the evolution of the electronic densities of the different phases in the samples (crystalline and amorphous phases) and, in particular, the evolution of the interphases between them, for dimensions ranging from ca. 50 to 500 Å. These dimensions correspond to the order of magnitude of crystalline lamellae and their stacks [40]. In Fig. 9, the evolutions of the intensities can be attributed to the density evolutions of the FE, DFE, RFE crystalline phases and of the amorphous phase. The steep drop observed in Fig. 9a and b has already been discussed in a previous study and can be interpreted as the disappearance of the FE phase [47]. Therefore, once again, three different behaviors can be observed for the three samples during heating: a sharp transition for Copo65-A-Pol at ca. 90 °C, a less steep transition at ca. 85 °C for Copo65-A, and a continuous transition for Copo46-A. During the cooling ramp, the evolutions for Copo65-A-Pol and Copo65-A are very similar and show once again that the heating above T_C erases the remnant polarization. Their Curie transition is at ca. 65 °C, while Copo46-A has a continuous transition. A slight thermal hysteresis regarding the intensities can be observed for Copo46-A. This hysteresis was already observed on the DSC thermograms (Fig. 7b) and by dielectric spectroscopy (Fig. 1b), but can be also attributed to physical ageing of the amorphous phase which disappears after the first heating above T_C. The intensity of the SAXS signal evolves with the density contrast between the crystalline and the amorphous phases, which increases after rejuvenation of the amorphous phase.

3.3.3. *Solid-state NMR*

The monitoring of the MAS ^{19}F SS-NMR spectra of the copolymers upon heating and cooling between 20 and 100 °C was performed to investigate the effect of temperature on the NMR spectra. Figs. 10 and 11 show the evolution of DP ^{19}F spectra in the CF_2 region for Copo65-A, Copo65-A-Pol and Copo46-A as a function of temperature upon heating and cooling.

For both Copo65 samples, temperature-dependent analyses of the spectra (Fig. 10) show that the signals, 1′ to 10′, associated with conformations in crystal disappear. This disappearance occurs at around 65-70 °C for Copo-65-A and at around 70-75 °C for Copo65-A-Pol, as highlighted in Fig. 10 by thicker lines. The deconvolutions of the spectra in the next section will highlight the intensities of these signals, 1′ to 10′, and give more precise disappearance temperatures. Upon cooling, these conformation signals reappear at around 50 °C for both Copo65-A and Copo65-A-Pol. In contrast, for Copo46-A (Fig. 11), the line widths of the spectra decrease with increasing temperature, but no signal appears or disappears. This evolution of the spectrum is reversible without hysteresis upon cooling from 100 to 20 °C, as shown in Fig. 11.

For the three samples, the peak around −106 ppm (noted peak S in Fig. 11) shows a peculiar behavior. From around 50 °C, a shoulder appears downfield and increases in intensity with increasing temperature. Aimi et al. reported this behavior and ascribed this change in the ^{19}F NMR spectra to the presence of two mobile phases at high temperature [29,30]. These signals which correspond to the CF_2 motif of the VDF unit in a VDF-TrFE/HT junction were indeed assigned by Aimi et al. to the amorphous and the paraelectric phases. Looking into the shoulder observed at 100 °C (peaks at −104.4 and −106.0 ppm, denoted S in Fig. 11), two possible interpretations can be proposed. (1) This is simply caused by a gain in resolution at this temperature, which is closer to that of solution NMR spectroscopy. Indeed, the solution NMR spectrum shows a high-intensity doublet (assigned to two doublets of non-equivalent fluorines at −106.2 and −107.8 ppm) similar to what can be observed in the SS-NMR spectrum at 100 °C. (2) This is caused by the paraelectric phase, which emerges with a slightly different isotropic

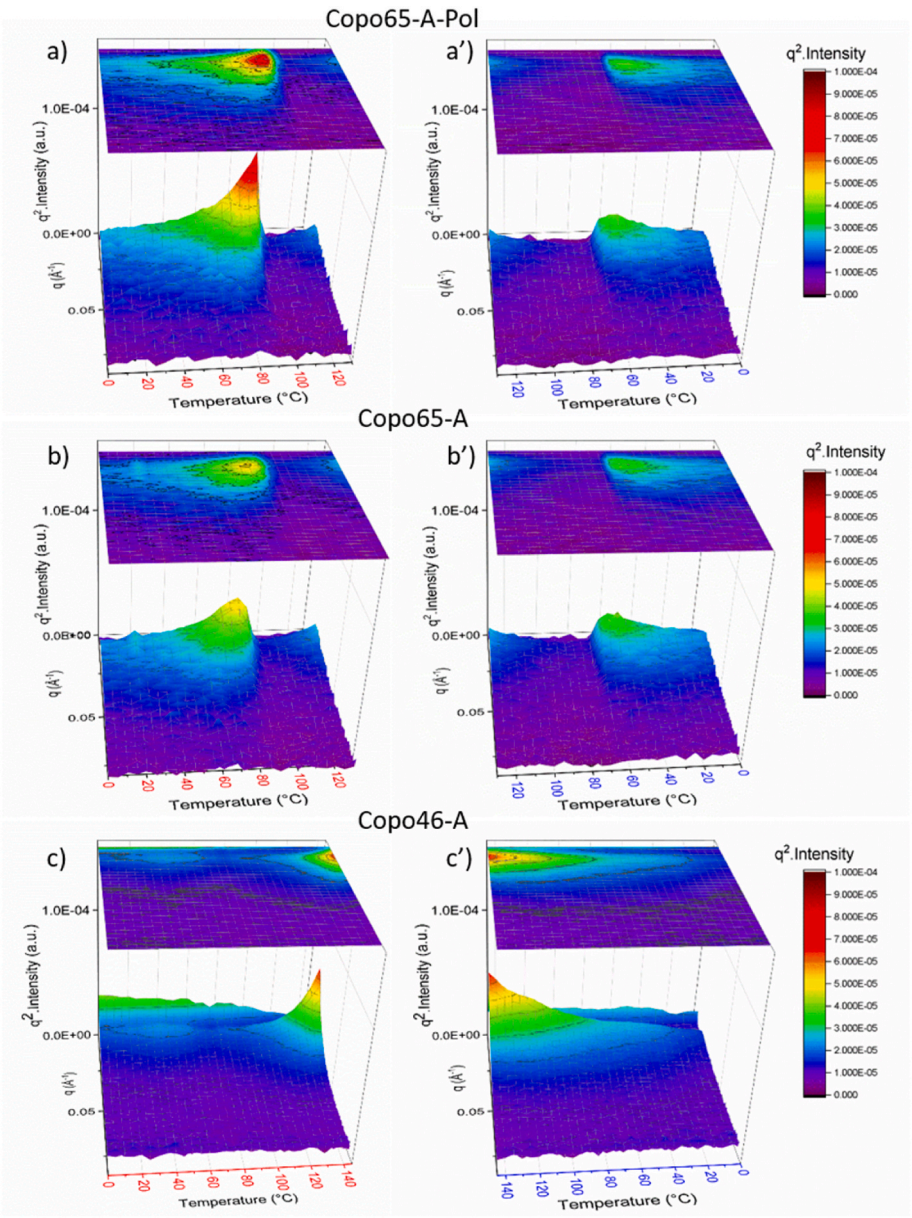

Fig. 9. 3D representation of the in-situ SAXS spectra $q^2I(q)$ recorded on a), a') Copo65-A-Pol, b), b') Copo65-A and c), c') Copo46-A during a), b), c) heating to the annealing temperature and a'), b'), c') cooling until 0 °C.

chemical shift value to that of the amorphous phase. The only way to verify this phenomenon would have been to carry out experiments at higher temperatures to see if two distinct peaks were obtained. Unfortunately, it was not possible to further increase the temperature with our instruments.

Fig. 12 shows the evolution of peak intensities through deconvolution as a function of temperature. T_D represents the temperature at which the peak disappears upon heating and T_A corresponds to the temperature at which the peak reappears during cooling.

For Copo65-A (Fig. 12a), the different peaks disappear at temperatures ranging from 80 to 100 °C. After polarization (Fig. 12b), an increase in the disappearance temperature of peaks 2′, 3′, and 4′ is observed. This change suggests that the crystals evolve toward a more "perfect" state, which disappears at higher temperatures. This observation could correspond to the NMR visualization of the polarization of the DFE phase transforming into the FE phase. Copo65-A and Copo65-A-Pol exhibit similar behavior during cooling, most bands start to reappear at the same temperatures (60, 70 and 80 °C) (Fig. SI–9). A thermal hysteresis is observed between heating and cooling for both Copo65-A and Copo65-A-Pol and its value is higher for Copo65-A-Pol. These observations confirm that these motifs are mainly located in the ferroelectric phase, which undergoes a transition to the paraelectric phase at T_C.

4. Discussion

In this section, SAXS-WAXS and NMR results are combined to obtain a more comprehensive insight of the static and dynamic behavior of the analyzed P(VDF-*co*-TrFE) copolymers. First, the WAXS and SAXS experiments presented in this study led to a structural comparison of the P(VDF-*co*-TrFE) samples. These results were complemented by NMR analysis, which enabled the identification of the motifs distributions between crystalline and amorphous phases and provided an estimation of the mobility of the motifs within the crystalline phases.

At room temperature, Copo65-A and Copo65-A-Pol consist of two crystalline phases (FE and DFE) and one amorphous phase. The ratios of

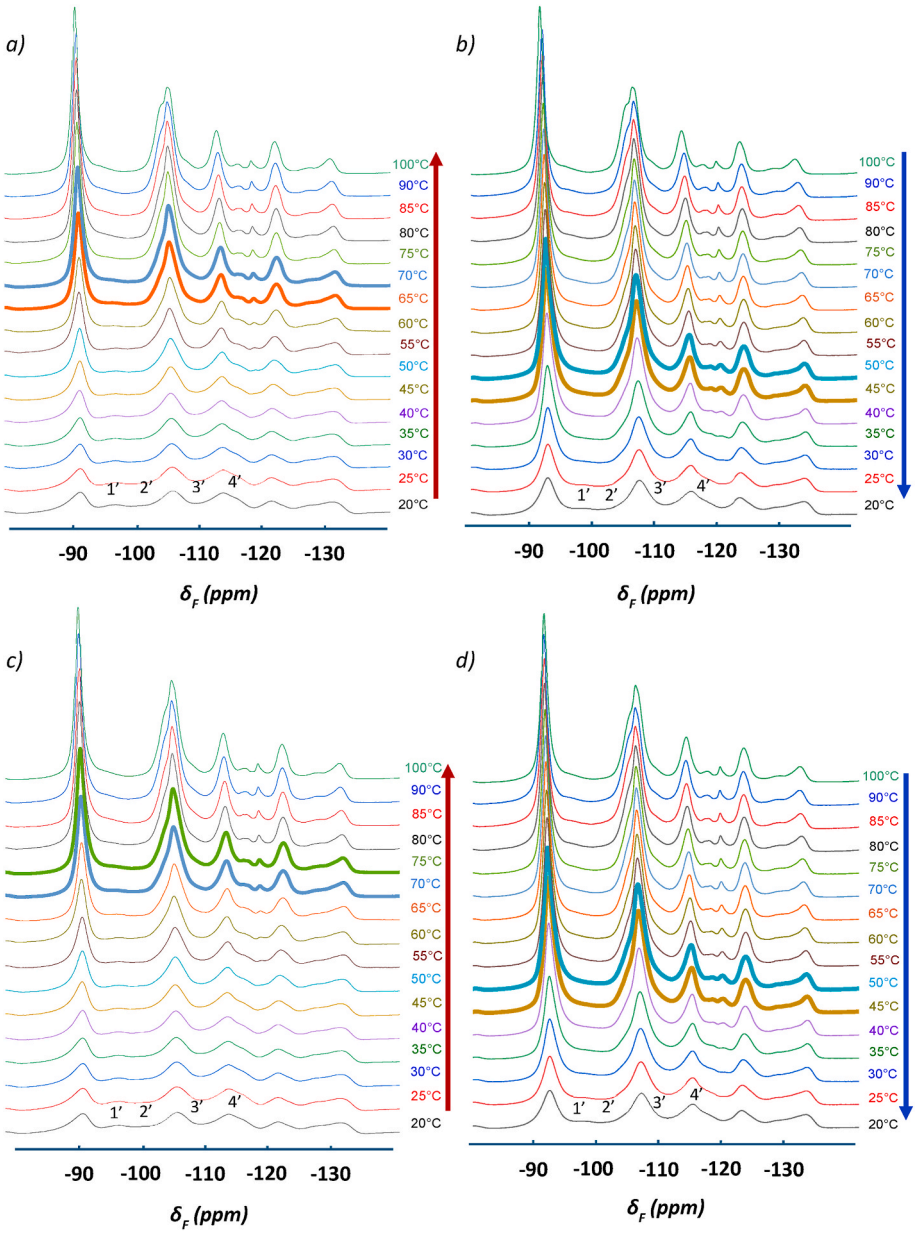

Fig. 10. Evolution of ^{19}F 576 MHz NMR DP spectra in the CF_2 region upon heating (a, c) and cooling (b, d) between 20 and 100 °C for a), b) Copo65-A and c), d) Copo65-A-Pol. The peaks 1′, 2′, 3′ and 4′ are identified on each spectrum at 20 °C.

these phases, obtained from WAXS spectra (Table 3), evolve after polarization, with the FE fraction increasing from 46% to 93%. The SAXS spectra associated with these samples highlight the presence of semi-crystalline structures made of alternated crystalline lamellae and amorphous interlayers. In parallel, the SS-NMR measurements showed that, for both Copo65-A and Copo65-A-Pol the FE and DFE crystalline fractions are associated with the 1′-10′ contributions, characterized by long $T_{1\rho}^{F}$ values and a mono-exponential behavior. It must be pointed out that the $T_{1\rho}^{F}$ values are consistently higher for Copo65-A-Pol, indicating a reduced mobility inside its crystalline phases compared to Copo65-A. Despite the fact that WAXS proves the presence of FE and DFE crystalline phases in the sample, they are undistinguishable by SS-NMR. An average $T_{1\rho}^{F}$ value is assigned to this mixture of DFE and FE crystalline phases. The longer $T_{1\rho}^{F}$ values for Copo65-A-Pol is consistent with the higher fraction of FE phase with respect to Copo65-A, as highlighted by WAXS.

The crystalline structure of Copo46-A at room temperature resulted to be strongly different from the other two samples. Only one crystalline phase (the RFE one) and the amorphous phase were detected by WAXS. The corresponding SAXS spectrum shows the existence of a periodic semi-crystalline organization. By SS-NMR, no crystalline phase was identified. The biexponential behaviors of 1, 9, and 10 contributions are associated with both the RFE and amorphous phase. This indicates that the characteristic motion of the RFE crystalline phase, which is known to contain a high density of conformational defects, is very close to the motion of the amorphous phase. The shorter relaxation time of the RFE phase compared to the FE and DFE phases is in good agreement with the WAXS results, which reveal the loss of the intra-chain order and higher inter-planar distances (inter-chain distance), i.e. larger crystalline lattice for the RFE phase than for the FE and DFE phases. It is probably this high mobility that makes the RFE phase non-polarizable.

In-situ measurements during a heating ramp were performed to study the behavior of Copo65-A, Copo65-A-Pol, and Copo46-A in the vicinity of the crystal to condis-crystal transition. As detailed in the literature and presented in the introduction of this study, the condis phase is characterized by a long-range positional and orientational order

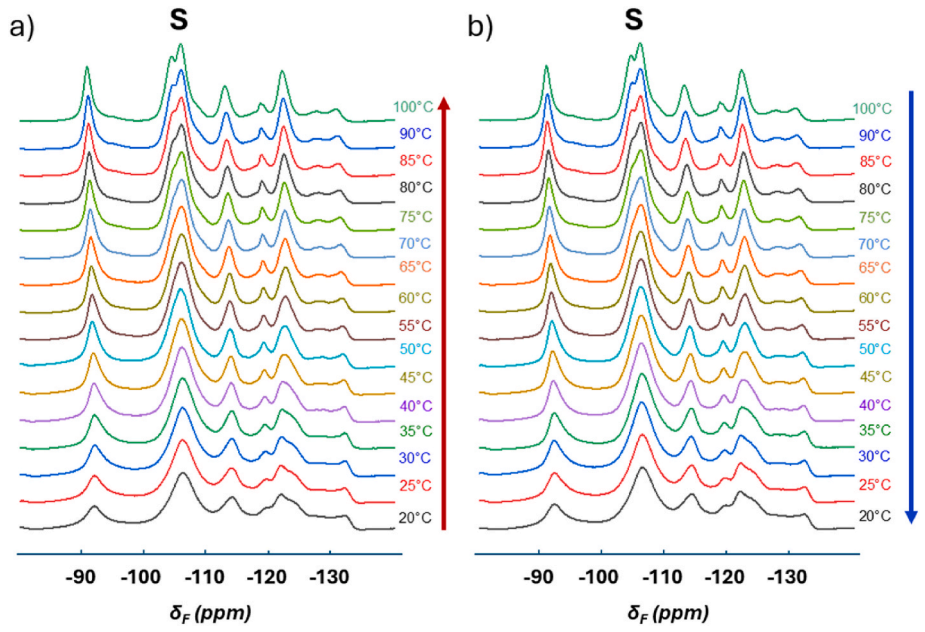

Fig. 11. Evolution between 20 °C and 100 °C of the CF_2 region of the ^{19}F 576 MHz NMR DP spectra of Copo46-A upon heating (a), upon cooling (b). The label S corresponds to the shoulder appearing next to the peak 2 at high temperature.

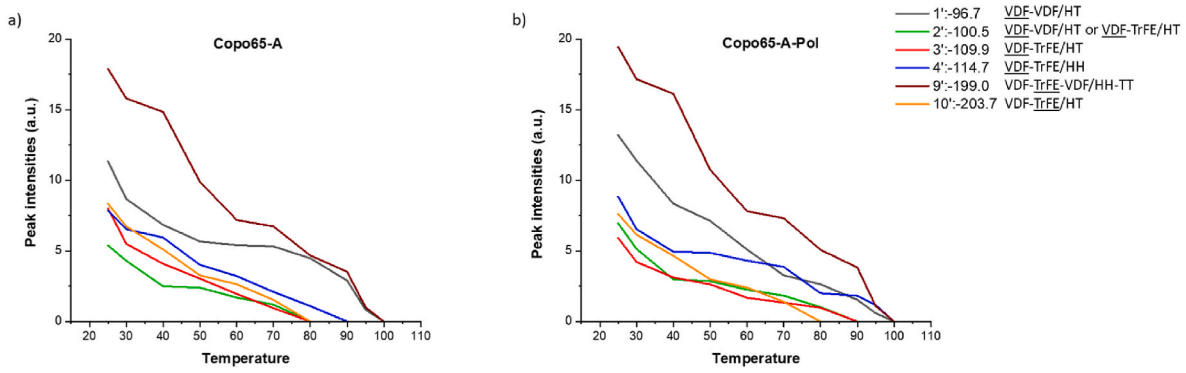

Fig. 12. Evolution upon heating of all conformation peaks (1′ to 10′) intensities on ^{19}F 576 MHz NMR DP experiment: a) in Copo65-A; (b) Copo65-A-Pol.

but with a dynamic conformational disorder, corresponding to the paraelectric phase of P(VDF-*co*-TrFE) copolymers. According to Wunderlich's study, depending on the concentration of conformational defects in the crystal fraction and on their tendency to aggregate, this transition can be either first-order (high aggregation tendency) or second-order (low aggregation tendency) [17].

In the present study, it was possible to detect and analyze the transition towards the condis phase with different techniques. First, DSC thermograms showed that Copo65-A and Copo65-A-Pol undergo a 1st order transition, evidenced by an enthalpic peak and by a marked thermal hysteresis. In-situ WAXS measurements illustrated the evolution of the inter-planar distances of the crystalline phases with temperature. The FE crystalline lattice showed a slighter expansion with respect to the crystalline phases which contain defects (DFE, RFE and PE). Once again, for Copo65-A and Copo65-A-Pol, a 1st order transition, characterized by the coexistence of the FE and PE phases within the thermal range of the transition and by a thermal hysteresis, was detected. This transition, commonly called Curie transition, is associated with the disappearance and reappearance (during the heating/cooling ramps) of the FE phase and consequently to the loss and recovery of the intra-chain order [47]. The transition of the DFE phase to the high temperature PE phase is continuous, when the temperature is high enough to promote the mobility of the polymer chains (ca. 50 °C). SAXS measurements further confirmed the discontinuous transition attributed to the 1st order transition (FE to PE during heating). The signal intensity, indicative of the electronic density difference between the crystal and amorphous phases, drops sharply for both Copo65-A-Pol and Copo65-A within the temperature range which corresponds to the disappearance of the FE phase [47].

This transition was also detected by SS-NMR measurements, for Copo65, which showed the disappearance and reappearance of NMR signals associated with the ferroelectric phase, as well as the thermal hysteresis. During the heating ramp, the NMR signals associated with the FE phase disappear at different temperatures. Although the measurements at room temperature cannot distinguish between the DFE and FE phases, the shift of the disappearance temperatures towards higher values can be interpreted by the DFE to FE transformation induced by polarization. These contributions disappear at T_C, suggesting that these motifs are the main components of the FE phase, while the study of the crystal to condis-phase transition for Copo46-A shows an overall continuous and reversible behavior with temperature.

Despite their different chemical composition and post-treatment, Copo65-A, Copo65-A-Pol, and Copo46-A have the same high temperature crystalline phase, namely the paraelectric or condis phase. This phase is characterized by a dynamic conformational disorder and a less dense crystalline lattice compared to the FE phase and to the low

temperature defective phases (DFE and RFE). At 100 °C, the highest temperature accessible for our SS-NMR setup, it is difficult to distinguish the contribution of the PE phase and of the amorphous phase. This could be explained by the temperature limit of the instrument (100 °C) or/and probably by the high mobility of the PE phase, very similar to that of the amorphous phase.

The present study showed the importance of coupling X-rays and NMR techniques. On the one hand, the NMR separate crystalline and amorphous phases which have significantly different mobilities. On the other hand, SAXS-WAXS measurements make it possible to distinguish between short-range (amorphous) and long-range (crystalline) order between chains. They also provide insight into the size of the crystalline lattices, reflecting the density of the different phases. Combining the two techniques enables the association of low-density crystalline phases with high molecular mobility.

As reminded in the introduction of this study, Wunderlich demonstrated that the crystal to condis-crystal transition can be of the first or the second order, at high or low aggregation tendency, respectively. The aggregation tendency is directly related to the intermolecular interactions between defect-free and defective chain segments and consequently plays a key role in governing the 1st or 2nd order nature of the crystal to condis-crystal transition. According to our results, the FE and DFE/RFE phases undergo a 1st and a 2nd order transition, respectively. This suggests that, at low concentration of conformational defects, these defects are rejected from the FE phase and consequently aggregate in the amorphous phase (1st order transition). At high concentration of conformational defects, they do not aggregate but instead are homogeneously included in the DFE or RFE crystal lattice. Consequently, interactions between defect-free and defective chain segments exist within the DFE and RFE crystals, and the transition to the PE phase occurs as a 2nd order transition. Therefore, the transitions observed in this study of the FE and RFE phases towards the condis phase are in accordance with the description made by Wunderlich.

5. Conclusion

In this article, various experimental techniques were used to probe the static (DSC, SAXS-WAXS) and dynamic (SS-NMR) behavior of fluorocopolymer chains located in amorphous and crystalline phases. This article presents the resulting study of the relationship between chain mobility and semi-crystalline organization of two P(VDF-*co*-TrFE) copolymers of 65/35 and 46/54 VDF/TrFE ratios. The FE and DFE crystalline phases (VDF/TrFE = 65/35) are the densest ones, characterized by low molecular mobility. The RFE (VDF/TrFE = 46/54) and PE (at high temperature) phases are less dense, without intra-chain order, and their high mobility is similar to the one of the amorphous phase. Interestingly, SS-NMR only detects crystalline phases constituted by a lattice ordered in the three directions. The loss of correlation along the polymer chains, deduced from SAXS-WAXS measurement, are interpreted by SS-NMR as a very mobile phase similar to the amorphous one. The joint WAXS and SS-NMR study allows for better specification of the DFE and RFE crystalline phases. The RFE phase is less dense, with higher interplanar distances [39], and with remarkably highly mobile chemical sequences, comparable to the amorphous phase. It is probably this mobility that makes this phase non-polarizable. Finally, the representation of the PE high temperature phase, obtained through a 1st or 2nd order transition (from the FE and RFE phases, respectively) was found to be consistent with the description of the conformationally disordered (condis) phase made by Wunderlich.

CRediT authorship contribution statement

Sara Zanchi: Writing – original draft, Investigation, Formal analysis, Data curation, Conceptualization. **Sami Zeliouche:** Writing – original draft, Investigation, Formal analysis, Data curation, Conceptualization. **Vincent Ladmiral:** Writing – review & editing, Supervision, Project administration, Methodology, Funding acquisition, Conceptualization. **Gilles Silly:** Writing – review & editing, Supervision, Methodology, Conceptualization. **Fabrice Domingues Dos Santos:** Writing – review & editing, Resources. **Béatrice Allard-Breton:** Writing – review & editing, Methodology. **Sylvie Tencé-Girault:** Writing – review & editing, Supervision, Methodology, Investigation, Formal analysis, Conceptualization. **Sébastien Roland:** Writing – review & editing, Supervision, Methodology, Investigation, Formal analysis, Conceptualization.

Declaration of competing interest

The authors declare that they have no known competing financial interests or personal relationships that could have appeared to influence the work reported in this paper.

Acknowledgments

This work was partially funded by the French National Research Agency (ANR FETA project, ANR-18-CE06-0024) and partially carried out within the framework of the Industrial Chair Arkema (Arkema/CNRS-ENSAM-Cnam, Arkema N° AC-2018-413, CNRS N° 183697). René-Paul Eustache (Arkema CERDATO, Serquigny), Ilias Iliopoulos (PIMM ENSAM), and Bruno Améduri (ICGM) are thanked for the stimulating discussions on NMR during the meetings of the FETA consortium. The authors are grateful to LEM laboratory (Arkema CERDATO, Serquigny) for the access to X-ray diffraction and dielectric spectroscopy facilities. The authors also thank Cédric Totée for his instrumental help with the technical aspect of the solid-state NMR spectroscopy. The authors would also like to thank Dr. Cédric Lorthioir (UMPC, Paris) for the very rich discussion that took place during Dr. Zeliouche's PhD viva.

Appendix A. Supplementary data

Supplementary data to this article can be found online at https://doi.org/10.1016/j.polymer.2026.129894.

Data availability

Data will be made available on request.

References

[1] A.J. Lovinger, Poly(vinylidene fluoride), in: Developments in Crystalline Polymers-1, Applied Science Publishers, 1982, pp. 195–273.
[2] H. Kawai, The piezoelectricity of Poly(vinylidene fluoride), Jpn. J. Appl. Phys. 8 (7) (1969) 975–976.
[3] R.G. Kepler, R.A. Anderson, Ferroelectricity in polyvinylidene fluoride, J. Appl. Phys. 49 (1978) 1232–1235.
[4] A.J. Lovinger, Ferroelectric polymers, Science 220 (4602) (1983) 1115–1121.
[5] J.B. Lando, W.W. Doll, The polymorphism of poly(vinylidene fluoride). I. The effect of head-to-head structure, J. Macromol. Sci., Part B: Phys. 2 (1968) 205–218.
[6] B.L. Farmer, A.J. Hopfinger, J.B. Lando, Polymorphism of poly(vinylidene fluoride): potential energy calculations of the effects of head-to-head units on the chain conformation and packing of poly(vinylidene fluoride), J. Appl. Phys. 43 (1972) 4293–4303.
[7] A.J. Lovinger, D.D. Davis, R.E. Cais, J.M. Kometani, The role of molecular defects on the structure and phase transitions of poly(vinylidene fluoride), Polymer 28 (1987) 617–626.
[8] T. Soulestin, V. Ladmiral, F. Domingues Dos Santos, B. Améduri, Vinylidene fluoride- and trifluoroethylene-containing fluorinatedelectroactive copolymers. How does chemistry impact properties? Prog. Polym. Sci. 72 (2017) 16–60.
[9] K. Tashiro, M. Kobayashi, Structural phase transition in ferroelectric fluorine polymers: X-ray diffraction and infrared/Raman spectroscopic study, Phase Transitions 18 (3-4) (1989) 213–246.
[10] F. Bargain, P. Panine, F. Domingues Dos Santos, S. Tencé-Girault, From solvent-cast to annealed and poled poly(VDF-co-TrFE) films: new insights on the defective ferroelectric phase, Polymer 105 (2016) 144–156.
[11] K. Tashiro, K. Takano, M. Kobayshi, Y. Chatani, H. Tadokoro, Structural study on ferroelectric phase transition of vinylidene fluoride-trifluoroethylene copolymers (III) dependence of transitional behavior on VDF molar content, Ferroelectrics 57 (1984) 297–326.

[12] D. Thuau, K. Kallitsis, S. Ha, F. Bargain, T. Soulestin, G. Pecastaings, S. Tencé-Girault, F. Domingues Dos Santos, G. Hadziioannou, High and temperature-independent dielectric constant dielectrics from PVDF-Based terpolymer and copolymer blends, Adv. Electron. Mater. (2020) 1901250.
[13] A.J. Lovinger, T. Furukawa, G.T. Davis, M.G. Broadhurst, Crystallographic changes characterizing the Curie transition in three ferroelectric copolymers of vinylidene fluoride and trifluoroethylene: 1. As-crystallized samples, Polymer 24 (1983) 1225–1232.
[14] A. Lovinger, T. Furukawa, G.T. Davis, M.G. Broadhurst, Crystallographic changes characterizing the Curie transition in three ferroelectric copolymers of vinylidene fluoride and trifluoroethylene: 2. Oriented or poled samples, Polymer 24 (1983) 1233–1239.
[15] K. Tashiro, R. Tanaka, Structural correlation between crystal lattice and lamellar morphology in the ferroelectric phase transition of vinylidene fluoride–trifluoroethylene copolymers as revealed by the simultaneous measurements of wide-angle and small-angle X-ray scatterings, Polymer 47 (2006) 5433–5444.
[16] G. Teyssedre, A. Bernes, C. Lacabanne, Cooperative movements associated with the curie transition in P(VDF-TrFE) copolymers, J. Polym. Sci., Part B: Polym. Phys. 33 (1995) 879–890.
[17] B. Wunderlich, M. Möller, J. Grebowicz, H. Baur, Conformational motion and disorder in low and high molecular mass crystals, Adv. Polym. Sci. 87 (1988) 1–121.
[18] G. Ungar, Thermotropic hexagonal phases in polymers: common features and classification, Polymer 34 (1993) 2050–2059.
[19] H. Baur, Phase transitions : condis crystals, in: Thermophysics of Polymers I: Theory, Springer, 1999, pp. 297–336.
[20] E. Bellet-Amalric, J. Legrand, Crystalline structures and phase transition of the ferroelectric P(VDF-TrFE) copolymers, a neutron di, Eur. Phys. J. B 3 (1998) 225–236.
[21] R.R. Kolda, J.B. Lando, The effect of hydrogen-fluorine defects on the conformational energy of polytrifluoroethylene chains, J. Macromol. Sci., Part B: Phys. 11 (1975) 21–39.
[22] Y. Liu, H. Aziguli, B. Zhang, W. Xu, W. Lu, J. Bernholc, Q. Wang, Ferroelectric polymers exhibiting behaviour reminiscent of a morphotropic phase boundary, Nature 562 (2018) 96–100.
[23] C. Perry, E.A. Dratz, Y. Ke, J.M. Kometani, R.E. Cais, V.H. Schmidt, Ferroelectric transition in 70/30 VF2/TrFE copolymer studied by Deuteron nmr, Ferroelectrics 92 (1989) 55–63.
[24] K. Tashiro, Crystal structure and phase transition of PVDF and related copolymers, in: Ferroelectric Polymers : Chemistry, Physics, and Applications, Marcel Dekker, Inc., 1995, pp. 63–182.
[25] R. Su, J.-K. Tseng, M.-S. Lu, M. Lin, Q. Fu, L. Zhu, Ferroelectric behavior in the high temperature paraelectric phase in a poly(vinylidene fluoride-co-trifluoroethylene) random copolymer, Polymer 53 (2012) 728–739.
[26] K. Tashiro, H. Yamamoto, Structural evolution mechanism of crystalline polymers in the Isothermal Melt-Crystallization process: a proposition based on simultaneous WAXD/SAXS/FTIR measurements, Polymers 11 (2019) 1316.
[27] F. Ishii, A. Odajima, Proton spin lattice relaxation in vinylidene Fluoride/Trifluoroethylene copolymer I. Vinylidene fluoride 72 mol% copolymer, Polym. J. 18 (7) (1986) 539–546.
[28] F. Ishii, A. Odajima, Proton spin lattice relaxation in vinylidene Fluoride/Trifluoroethylene copolymers II. Effects of vinylidene fluoride content upon spin relaxation processes, Polym. J. 18 (7) (1986) 547–555.
[29] K. Aimi, S. Ando, P. Avalle, R.K. Harris, Solid-state 19F MAS and 1H ! 19F CP/MAS NMR study of the phase transition behavior of vinylidene fluoride–trifluoroethylene copolymers: 1. Uniaxially drawn films of VDF 75% copolymer, Polymer 45 (2004) 2281–2290.
[30] K. Aimi, S. Ando, Solid-state 19F MAS and 1H-19F CP/MAS NMR study of the phase-transition behavior of vinylidene fluoride–trifluoroethylene copolymers: 2. Semi-crystalline films of VDF 75% copolymer, Polym. J. 44 (2012) 786–794.
[31] F. Ishii, A. Odajima, Ferroelectric transition in vinylidene fluoride and trifluoroethylene copolymers studied by NMR method II. 52 and 65 mol% vinylidene fluoride copolymers, Polym. J. 23 (8) (1991) 999–1008.
[32] V.I. Sultanov, V.V. Atrazhev, D.V. Dmitriev, N.S. Erikhman, D.U. Furrer, S. F. Burlatsky, Microscopic mechanism of the large electrocaloric effect in vinylidene difluoride-based polymers, Macromolecules 54 (2021) 3744–3754.
[33] Foxtrot software can be obtained by sending a mail to foxtrot@xenocs.*com*. Software is Free for Non-profit Usage, Directly Useable with Nexus and ESRF 2D Data Format.
[34] M. Wojdyr, Fityk: a general-purpose peak fitting program, J. Appl. Crystallogr. 43 (5) (2010) 1126–1128.
[35] D. Massiot, F. Fayon, M. Capron, I. King, S. Le Calvé, B. Alonso, J.-O. Durand, B. Bujoli, Z. Gan, G. Hoastson, Modelling one- and two-dimensional solid-state NMR spectra, Magn. Reson. Chem. 40 (2002) 70–76.
[36] Q.M. Zhang, V. Barthi, X. Zhao, Giant electrostriction and relaxor ferroelectric behaviour in electron-irradiated poly(vinylidene fluoride-trifluoroethylene) copolymer, Science 280 (1998) 2101–2104.
[37] S. Zhang, R.J. Klein, K. Ren, B. Chu, X. Zhang, J. Runt, Normal ferroelectric to ferroelectric relaxor conversion in fluorinated polymers and the relaxor dynamics, J. Mater. Sci. 41 (2006) 271–280.
[38] L. Yang, B.A. Tyburski, F. Domingues Dos Santos, M.K. Endoh, T. Koga, D. Huang, Y. Wang, L. Zhu, Relaxor ferroelectric behavior from strong physical pinning in a Poly(vinylidene fluoride-co-trifluoroethylene-co-chlorotrifluoroethylene) random terpolymer, Macromolecules 47 (2014) 8119–8125.
[39] F. Bargain, D. Thuau, G. Hadziioannou, F. Domingues Dos Santos, S. Tencé-Girault, Phase diagram of poly(VDF-ter-TrFE-ter-CTFE) copolymers: relationship between crystalline structure and material properties, Polymer 213 (2021) 123203.
[40] S. Zanchi, M. Engel, A. Pascaud, F. Bargain, S. Lebreton, F. Domingues dos Santos, S. Roland, S. Tencé-Girault, Combination of AFM and SAXS studies for semi-crystalline morphologies: focus on P(VDF-ter-TrFE-ter-CTFE) terpolymers, Polym. Test. 120 (2023) 107973.
[41] P.-Y. Mabboux, K.K. Gleason, 19F NMR characterization of electron beam irradiated vinylidene fluoride-trifluoroethylene copolymers, J. Fluor. Chem. 113 (2002) 27–35.
[42] S. Ando, R.K. Harris, S.A. Reinsberg, Solid-state 1H → 19F/19F → 1H CP/MAS NMR study of poly(vinylidene fluoride), Magn. Reson. Chem. 40 (2002) 97–106.
[43] P. Wormald, B. Ameduri, R.K. Harris, P. Hazendonk, Fluorine-19 solid state NMR study of vinylidenefluoride polymers using selective relaxation filters, Solid State Nucl. Magn. Reson. 30 (2006) 114–123.
[44] P. Holstein, U. Scheler, R.K. Harris, Semicrystallinity and polymorphism in PVDF: a solid-state 19F n.m.r. investigation, Polymer 39 (1998) 4937–4941.
[45] P. Wormald, D.C. Apperley, F. Beaume, R.K. Harris, Fluorine-19 solid-state NMR investigation of regiodefective semicrystalline α-poly(vinylidenefluoride), Polymer 44 (2003) 643–651.
[46] P. Wormald, Nuclear Magnetic Resonance Spectroscopy of Vinylidenefluoride Polymers, University of Durham, 2005. PhD Dissertation.
[47] F. Bargain, D. Thuau, P. Panine, G. Hadziioannou, F. Domingues Dos Santos, S. Tencé-Girault, Thermal behavior of poly(VDF-ter-TrFE-ter-CTFE) copolymers: influence of CTFE termonomer on the crystal-crystal transitions, Polymer 161 (2019) 64–77.